Tribology Letters (2018) 66:153
https://doi.org/10.1007/s11249-018-1107-x

ORIGINAL PAPER

Characterization of DLC-Coated and Uncoated Surfaces by New Directional Blanket Curvature Covering (DBCC) Method

Marcin Wolski[1] · Pawel Podsiadlo[1] · Gwidon W. Stachowiak[1] · Kenneth Holmberg[2] · Anssi Laukkanen[2] · Helena Ronkainen[2]

Received: 9 August 2018 / Accepted: 23 October 2018 / Published online: 3 November 2018

Abstract

Roughness and curvature of diamond-like carbon (DLC) surface coatings change with both scale and direction of a measurement. However, the changes are not detected by currently used standard parameters which are designed to work with isotropic surfaces at a single scale, thus providing only a limited information about multiscale and directional roughness and curvature. The problem of detailed roughness characterization of DLC-coated surfaces has been addressed in our previous work [Wolski et al. Multiscale characterization of 3D surface topography of DLC-coated and uncoated surfaces by directional blanket covering method. Wear 2017:388–389:47–56]. However, surface curvature description still remains an unresolved issue. To overcome this shortcoming, a directional blanket curvature covering (DBCC) method was developed. The method calculates curvature, peak and valley dimensions which quantify multiscale and directional curvature complexity of surface topography, peaks and valleys, respectively. Higher values of the dimensions represent higher complexity. In the current study, the DBCC method was used to analyse DLC-coated and uncoated bearing steel samples with increasing roughness and curvature. Its ability to discriminate between these two groups of surfaces was evaluated. Results showed that the method could detect minute changes in surface curvature at individual scales and directions. The method would be of interest to those who design wear-resistant systems and surfaces.

Keywords DLC coatings · Surface characterization · Curvature

Nomenclature

Abbreviations

a-C	Amorphous carbon
CD, PD, VD	Curvature, peak and valley dimensions
CS, PS, VS	Curvature, peak and valley signatures
DBC	Directional blanket covering
DBCC	Directional blanket curvature covering
DLC	Diamond-like carbon
DLC-S, DLC-A, DLC-R	Smooth, average and rough DLC-coated surfaces
FD	Fractal dimension
FS	Fractal signature
ISO	International Organization for Standardization
NaN	Not-a-number
SD	Standard deviation
SE	Structuring element
STE-S, STE-A, STE-R	Smooth, average and rough uncoated surfaces

Symbols

a	Coefficient of a quadratic polynomial
ε	Scale
κ	Curvature
N	Number of pixels
P	Statistical significance
Sa (μm)	Arithmetic mean height
Sds (pks/mm^2)	Density of peaks
Ssc (1/mm)	Mean curvature of summits
θ (degree)	Direction

✉ Marcin Wolski
marcin.wolski@curtin.edu.au

[1] Tribology Laboratory, School of Civil and Mechanical Engineering, Curtin University, GPO Box U1987, Perth, WA 6845, Australia

[2] VTT Technical Research Centre, Espoo, Finland

Subscripts

1, 2, 3	Indices
0, 45, 90	Horizontal, diagonal and vertical directions
S, *M*, *L*	Small, medium and large scales
Sta	Texture minor axis
Str	Texture aspect ratio
x, *y*	Horizontal and vertical coordinates
w, *h*	Width and height

1 Introduction

Roughness (i.e. fine texture irregularities) and curvature (i.e. the amount of a surface bend from a plane at a particular point) of diamond-like carbon (DLC)-coated surfaces have been characterized using standard ISO parameters. For example, arithmetical mean height (Sa) and arithmetic mean peak/summit curvature (Spc/Ssc) parameters were used to study effects of roughness and curvature of DLC-coated injection cams on friction and wear in a truck engine [1]. These two parameters and a root-mean-square roughness (Sq) parameter were also used to study effects of surface topography on friction and wear behaviour of DLC coatings in hermetic compressors and to investigate the microbe adhesion and biofilm formation on stainless steel plates coated with DLC [2, 3]. Other investigations focus on effects of thin lubricants on topography and adhesion of DLC coated ultra-high density hard discs and the control of flash temperature in sliding contacts [4–6].

Although the standard surface characterization parameters are useful, their application is limited. As single and average values are calculated for an entire surface texture, the parameters do not account for the multiscale and anisotropic nature of DLC surfaces [7–9], i.e. changes in roughness and curvature at different scales and directions. Therefore, new parameters and methods that can provide the detailed information about DLC surface topography are required.

An initial attempt to solve the issue of directional and multiscale roughness characterization of DLC-coated surfaces was through the variance orientation transform (VOT) method [7]. The VOT method calculates fractal signatures (FSs) in different directions [10]. A FS is a set of fractal dimensions (FDs) calculated at individual scales and a FD is the most popular fractal measure of a surface roughness. Higher values of FD mean rougher texture. Despite promising results obtained in characterization of engineering surfaces (including DLC) [7, 11, 12], and even medical [13–15] textures, important limitations of the method have been identified. Namely, it does not automatically determine scales of calculations and it is dependent on the Brownian fractal motion condition. This condition is relatively strict, often not met by engineering surfaces, since it is satisfied when (i) grey-scale level differences calculated at different pixel distances for a surface image are normally distributed, and (ii) a log–log plot of variances of the differences against the distances is a straight line [16]. In order to overcome these limitations, a directional blanket covering (DBC) method was developed [17]. The method has been successfully tested on DLC-coated and uncoated surfaces [8], detecting minute dissimilarities in FSs between the surfaces. In other study, strong correlations were found between directional FSs and wear and friction characteristics of DLC-coated surfaces using multiscale numerical finite element (FE) models [9]. It was demonstrated that the FSs relate to surface cracking, plastic deformations, local stress–strain and initiation of defects on DLC-coated surfaces at contact [9]. The contribution of surface topography features to the cracking and deformations was estimated to be $<40\%$. These studies could be complemented with characterization of surface curvature. However, a detailed multiscale curvature characterization still remains an unresolved problem. For example, so far, multiscale curvature analysis has been limited only to two directions, while the real surfaces can change in many directions [18].

The problem could be addressed by recently developed directional blanket covering curvature (DBCC) method [19]. The method provides sets of curvature (CD), peak (PD) and valley (VD) dimensions over a range of scales in different directions. In the method, the range of scales is automatically calculated for each surface texture image (spanning from the instrument resolution to 1/10 of the image shortest size), while the directions are chosen by the user. Also, the method is independent of the Brownian condition, i.e. the condition that grey-scale level differences are normally distributed and the log–log plot of variances of the differences against distances follows a straight line [19]. Curvatures are calculated for local surface profiles of different lengths (scales) and orientations which are extracted from the surface 3D height image (called range-image). Using the profile curvatures, a curvature matrix is first constructed for each scale and direction and then CDs, PDs and VDs are obtained. The dimensions quantify the curvature complexity (i.e. the amount of space filling with peaks and valleys over the unit area) of surface topography (CD), peaks (PD) and valleys (VD) at individual scales and directions. Higher values of the dimensions represent higher complexity. The DBCC method has so far been successfully used in characterization of isotropic computer-generated surfaces with increasing curvature complexity, anisotropic surfaces with varying curvature complexity with direction, and also, isotropic and anisotropic titanium alloy plates [19]. However, its usefulness in the characterization of DLC-coated surfaces has not yet been evaluated.

The aim of the current study is to evaluate the performance of the method in curvature characterization of DLC-coated surfaces. The evaluation is conducted using microscopic range-images of three bearing steel discs with increasing roughness and curvature (100 images per disc were obtained) with and without DLC coatings, respectively. Differences in curvature complexity between the uncoated and coated surfaces were investigated using statistical analyses.

2 Materials and Methods

2.1 The DBCC Method

The method calculates CDs, PDs and VDs at individual scales in different directions. In this section, steps for calculation of the dimensions are briefly described as they are presented in detail in Podsiadlo et al. [19].

1. A square grid of size of $N_w \times N_h$ pixels is generated and placed over the surface image in such a way that the grid and image are concentric and their borders are parallel (Fig. 1a, b). N_w and N_h are equal to the number of surface image pixels in the horizontal (N_x) and vertical (N_y) directions, respectively.
2. The grid rotates around its centre (Fig. 1c) by predefined directions θ (e.g. θ ranges from 0° to 180° in steps of 5°). Directions are measured with respect to the image horizontal axis. For $0° \le \theta \le 90°$, the grid size of $N_w \times N_h$ is automatically adjusted to ensure that all surface image pixels are covered using the following formulas [16]:

$$N_w = \left|\left(\text{floor}\left(N_x \cos(\theta) + N_y \sin(\theta)\right)\right)\right|$$

$$N_h = \left|\left(\text{floor}\left(N_x \sin(\theta) + N_y \cos(\theta)\right)\right)\right|.$$

   For the remaining directions (i.e. $90° < \theta < 180°$), a negative value of $\boldsymbol{\theta}$ is used in the above formulas.
3. For each rotation, a new image of size of $N_w \times N_h$ pixels (called rotated image) is generated. Initial values of the image are set to NaN (i.e. not-a-number). Grey-scale level values of surface image pixels covered by the grid are then copied into the rotated image (Fig. 1d) using a procedure detailed in [20]. Since the rotated image is generally larger than the surface image, some of its values remain NaNs. These values are not used in the subsequent calculations.
4. Local grey-scale level surface profiles are extracted from the rotated image using horizontal line structuring elements (SEs) of different lengths (Fig. 1d). SE length relates to scale ε as $2 \times \varepsilon + 1$. The scales lie between a surface topography measuring instrument's spatial resolution and $N_x/10$ (or $N_y/10$ if $N_y < N_x$). The smallest scale is determined by the instrument spatial resolution while the largest (i.e. 1/10 of the short size of surface image) is based on the Rank Taylor Hobson empirical criterion [19]. According to the criterion, a sampling length should include about ten whole roughness marks [21, 22].
5. A quadratic polynomial $f(x) = a_0 + a_1 x + a_2 x^2$ is fitted to each profile (Fig. 1e). The fitting was performed using the least square method. The method represents the best trade-off between accuracy and computational complexity [23]. The curvature κ of the polynomial is calculated as $\kappa = 2a_2 / \left(1 + a_1^2\right)^{\frac{3}{2}}$.
6. An $N_w \times N_h$ matrix (called curvature matrix) with initial values set to NaN is generated. Absolute values of the curvatures calculated are stored in the matrix (Fig. 1f).
7. The matrix is dilated and eroded using the horizontal line SEs (Fig. 1h). NaN values still present in the matrix are ignored in the operations.
8. Differences between the dilated and eroded versions of the curvature matrix are calculated at each scale. The differences are called surface areas (Fig. 1h).
9. For each direction, log–log plots of the surface areas against scales are constructed (Fig. 1i). The log–log plot data points often do not follow the power law, instead they form a curve or change in a zigzag fashion. To quantify the changes, the data points are divided into subsets of five data points with a line fitted into each subset (Fig. 1i). The five points are a trade-off between the ability to quantify local changes and the minimization of the effects of local artefacts in image (e.g. noise, blur) [19].
10. At each scale, rose plots are constructed by plotting the CDs obtained in polar coordinates (Fig. 1j).

Other two dimensions are calculated in the same way, with the difference that in the step 6, negative (PD) or positive (VD) values of the curvatures are stored in the matrix (Fig. 1f). Sets of CDs, PDs and VDs calculated at individual scales are called curvature (CS), peak (PS) and valley (VS) signatures, respectively.

2.2 Curvature, Peak and Valley Texture Parameters

To each rose plot of the CDs, ellipses are fitted and the following texture parameters are calculated [19]:

- Texture major axis curvature signature (CS_{Sta}). The parameter is defined as the set of CD_{Sta} values obtained at individual scales. At each scale, CD_{Sta} is equal to the

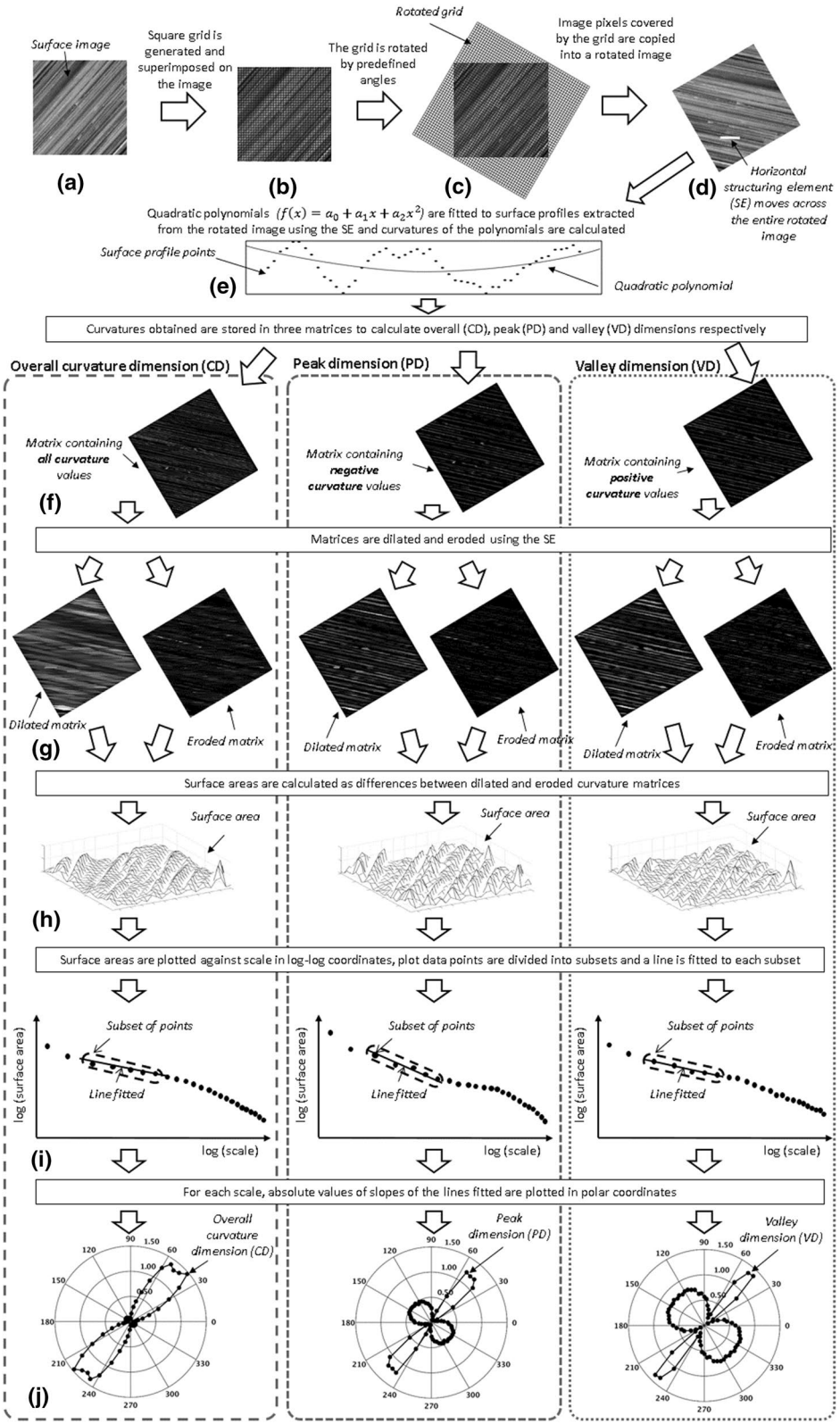

Fig. 1 Schematic illustration of the DBCC method: **a** surface image, **b** rotating grid superimposed on the image, **c** rotated grid, **d** rotated image, **e** surface profile, **f** curvature matrices, **g** dilated and eroded matrices, **h** surface areas, **i** log–log plots, and **j** rose plots

length of the major axis of the ellipse fitted and it represents dominating curvature component, i.e. a part of surface texture along direction with the most complex curvature.

- Texture aspect ratio curvature signature (CS_{Str}). The set of CD_{Str} values obtained at individual scales is calculated as the ratio of the minor to the major axes of the ellipses fitted. CD_{Str} takes values between 0 and 1. For surface textures exhibiting the same curvature complexity in all directions (i.e. isotropic surfaces), Str is equal to one. For anisotropic surfaces, Str is less than one.

Ellipses are also fitted to the rose plots of PDs and VDs, and texture major axis and aspect ratio signatures for peaks (PS_{Sta}, PS_{Str}) and valleys (VS_{Sta}, VS_{Str}) are calculated, respectively.

2.3 Example Applications of the DBCC Method

Two surfaces were analysed. The first surface was isotropic (Fig. 2a, c) and it was obtained by sandblasting, while the second surface (Fig. 2b, d) had anisotropy generated by rubbing a dry emery paper against the plate in one direction. 3D topography of each surface was measured using a chromatic confocal surface profilometer (AltiSurf 530, Altimet, France) with the lateral sampling intervals equal to 5 µm. The sampling area was 700 × 700 µm. The 3D surface data measured were encoded into 256 (140 × 140 pixels) grey-scale range-images. The direction of the grinding marks (i.e. 162°) on the anisotropic surface image was determined by averaging individual directions of ten lines manually drawn along the marks. Each direction was defined as an angle between the line drawn and the horizontal image axis.

The DBCC method was applied to the range-images of these surfaces, and the rose plots of CDs, PDs and VDs were constructed at scales ranging from 20 to 60 µm. Examples of the rose plots obtained are shown in Fig. 3. The figure shows directional changes of the overall surface curvature complexity (CD), and the curvature complexities of peaks (PD) and valleys (VD) at individual scales [19]. It can be seen from the figure that the plots obtained for the sandblasted surface exhibit a circular shape at all scales. In contrast, the plots constructed for the ground surface deviate considerably from the circular shape. These correctly indicate that the curvature of the sandblasted surface does not change considerably with direction, while the ground surface exhibits marked, directional curvature variations. This is further evidenced by the higher mean value of CS_{Str} (0.880) obtained for the sandblasted, as compared to the ground surface's value (0.825). Also, the mean value of

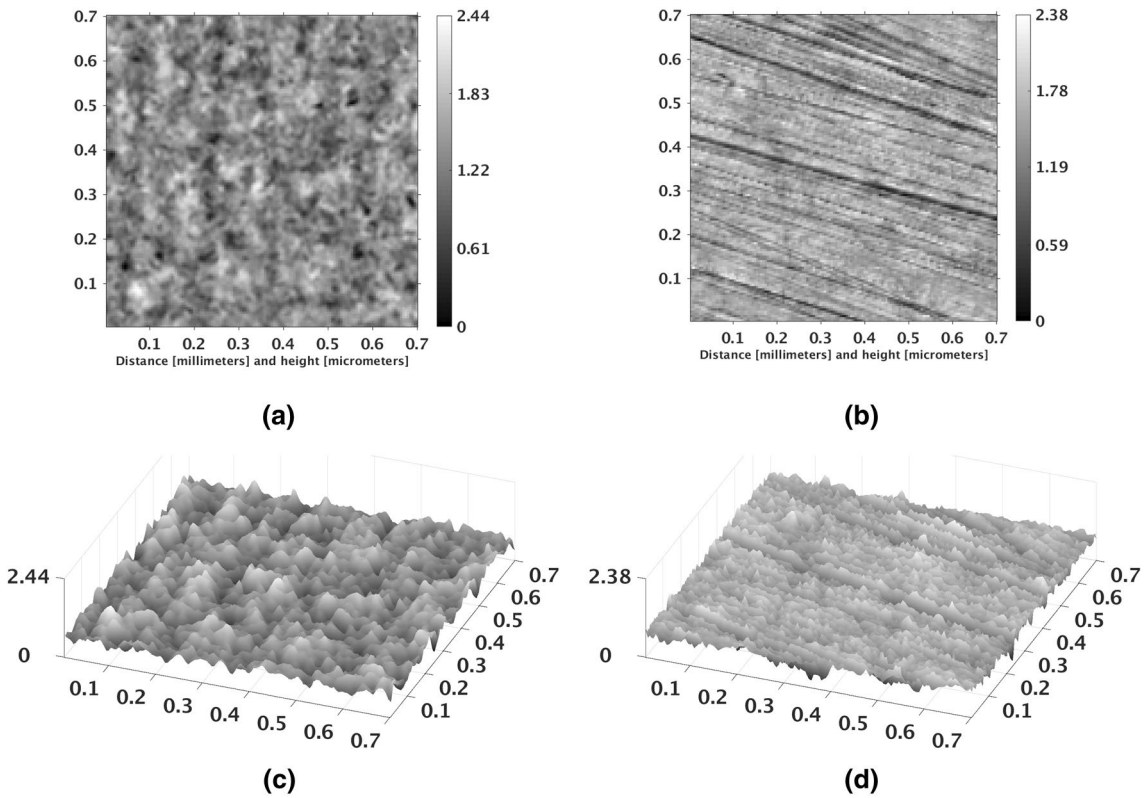

Fig. 2 Range-images of **a** sandblasted and **b** ground surfaces and **c**, **d** corresponding 3D views of the surfaces. Each image area is 0.7 × 0.7 mm

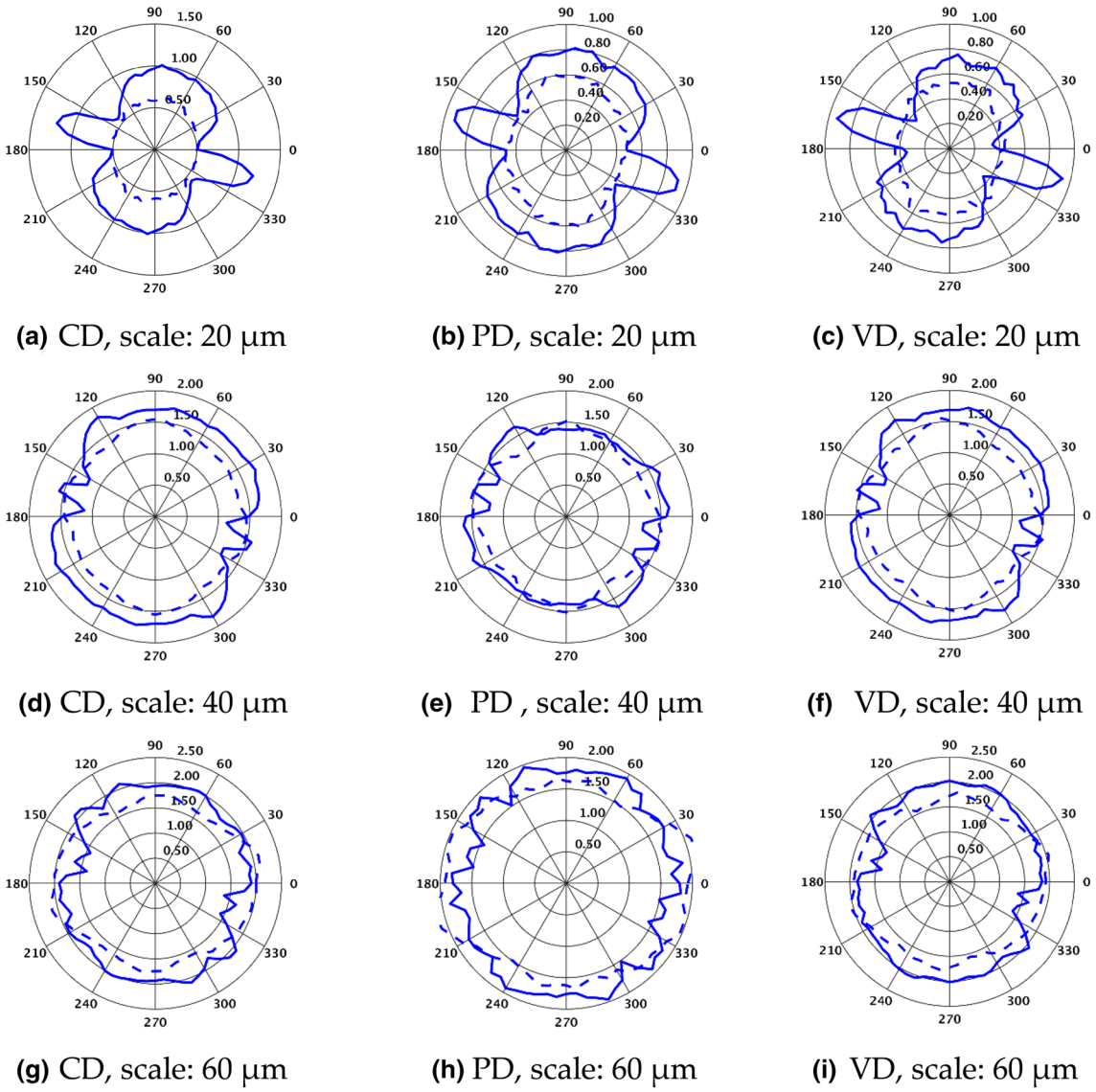

Fig. 3 Examples of rose plots of CDs, PDs and VDs obtained at scales of **a–c** 20 μm, **d–f** 40 μm and **g–i** 60 μm for the sandblasted (dashed line) and ground (solid line) surfaces shown in Fig. 2a, b, respectively

CS_{Sta} obtained for the ground surface (1.676) was higher than that for sandblasted surface (1.403). These results show that the grinding marks increase the complexity level of surface curvature.

At scales ranging from 20 to 25 μm, the plots obtained for the anisotropic surface show that CDs (Fig. 3a) are largest in 165° direction which is approximately the direction of grinding marks. Also, values of PDs and VDs obtained in this direction are similar, indicating that contributions of peaks and valleys to the overall curvature complexity are approximately equal (Fig. 3b, c). In contrast, PDs obtained in 75° direction, which is approximately the direction perpendicular to the grinding marks, are noticeably larger than VDs (Fig. 3b, c). This indicates that in the direction of 75° peaks contribute more to the overall curvature complexity as compared to valleys.

The above results indicate that there are equal numbers of small sharp peaks and valleys generated by rubbing along 165° direction and there are deformations of small peaks located between the grinding marks in the perpendicular direction of 75°.

For the scale range of 30–60 μm, CDs were largest (smallest) in about 75° (165°) direction and there were no marked differences between PDs and VDs (Fig. 3d–i). These indicate that the overall curvature of the anisotropic surface at these scales has the highest and lowest levels of complexity in 75° and 165°, respectively, and the contributions of peaks and valleys are approximately equal.

2.4 Uncoated and DLC-Coated Surfaces

Two groups of surface samples were used. In the first group, there were three bearing steel discs (AISI52100; diameter of 40 mm and thickness of 6 mm) ground in one direction [7]. Two discs were polished in such a way that one was smoother and less anisotropic than the other. The three discs are called smooth (STE-S), average (STE-A) and rough (STE-R), respectively. The STE-R represents the ground disc, while the STE-S and STE-A denote the two polished discs, respectively. The second group consisted of three hydrogen-free amorphous carbon (a-C) DLC-coated surfaces deposited on three steel discs of the same dimensions and type as the discs in the first group. The three discs were ground in one direction and two of them were also polished before the application of the coating [7]. The coatings (thickness ~ 1.7 µm) were deposited using a magnetron sputtering UDP650/6 system (Teer Coatings Limited, UK). The three DLC-coated discs are marked as smooth (DLC-S), average (DLC-A) and rough (DLC-R), respectively.

The 3D surface topography of all six discs was measured using the Altimet 530 surface profilometer. The surface scan areas were 10 × 10 mm with the lateral sampling intervals of 5 µm. Standard average roughness (Sa), density of summits (Sds) and mean summit curvature (Ssc) parameters were calculated for the surface areas scanned. Values of Sa obtained for the STE-S (DLC-S), STE-A (DLC-A) and STE-R (DLC-R) were 0.06 (0.14), 0.12 (0.47) and 0.23 (0.74), respectively. The Ssc took values of 0.009 (0.045) for the STE-S (DLC-S), 0.013 (0.058) for the STE-A (DLC-A) and 0.013 (0.042) for the STE-R (DLC-R). The Sds parameter was 639 (271), 27 (250) and 1320 (935), respectively. These values show that smooth, average and rough surfaces exhibit increasing roughness (i.e. increasing values of Sa). Also, the coated surfaces have smaller radii of curvature (i.e. larger values of Ssc) and a lower number of peaks/summits per unit area (i.e. lower values of Sds) than the uncoated surfaces. The exception is the DLC-A disc which has a higher number of peaks as compared to the STE-A.

The 3D elevation data obtained from the surface topography scans were encoded into range-images exhibiting 256 grey-scale level values (Fig. 4). Each range-image was split into 100 non-overlapping sub-images of size 200 × 200 pixels (i.e. 1 × 1 mm) resulting in 600 sub-images (i.e. 100 per surface).

2.5 The DBCC Method Setup

The DBCC method was applied to the sub-images of the coated and uncoated surfaces, and the CS_{Sta}, CS_{Str}, PS_{Sta}, PS_{Str}, VS_{Sta} and VS_{Str} parameters were calculated at 15 scales ranging from 0.20 to 0.90 µm in step of 5 µm. CSs, PSs and VSs were also calculated at the same scales in directions perpendicular (0°), diagonal (45°) and along (90°) the grinding marks, respectively. The reason is that these directions have been used in our previous study on wear and friction characteristics of DLC-coated surfaces [7–9]. The CSs (PSs, VSs) calculated in 0° direction are denoted as CS_0 (PS_0, VS_0), 45° as CS_{45} (PS_{45}, VS_{45}) and 90° as CS_{90} (PS_{90}, VS_{90}), respectively. Fifteen signature parameters were obtained per sub-image.

The scale range of CS_0 was divided into three intervals, i.e. small (0.20–0.40 µm), medium (0.45–0.65 µm) and large (0.70–0.90 µm). Values of CDs obtained for each interval were averaged, resulting in three parameters per sub-image, i.e., CD_{0_S}, CD_{0_M} and CD_{0_L}. The first and second subscripts denote the direction and interval of scale of calculations, respectively.

The interval averaged parameters were also calculated for PS_0, VS_0, CS_{45}, PS_{45}, VS_{45}, CS_{90}, PS_{90}, VS_{90}, CS_{Sta}, PS_{Sta}, VS_{Sta}, CS_{Str}, PS_{Str}, VS_{Str}.

2.6 Statistical Analysis

Shapiro–Wilk tests were used to check normality of the texture parameters calculated and P values less than 0.01 were considered as statistically significant. Unpaired student t-tests ($P \leq 0.05$, Mann–Whitney U whenever appropriate) were used to compare mean values of the parameters obtained for the sub-images of coated and uncoated surfaces. A power analysis was used to determine how many images are required to achieve a statistical power of 80%. The statistical analyses were performed using SPSS Statistics 21 (IBM, Corporation, Somers, NY) and G*Power 3 [24].

3 Results

Power analysis showed that at least 57 images are required per disc to detect a standardized effect size of 0.8 with power of 80% and $P = 0.001$. The mean ± standard deviations (SDs) obtained for the parameters calculated for the coated and uncoated surfaces at small, medium and large scales are plotted in Figs. 5, 6, 7.

3.1 STE-S and DLC-S Surfaces

The CS_{Sta}, PS_{Sta} and VS_{Sta} parameters calculated for the STE-S images were significantly higher ($P < 0.021$) than those for the DLC-S images at all scales (Fig. 5a–c). Same results were obtained for the CS, PS and VS calculated in 45° and 90° directions (Fig. 5d–i) and for the CS_0, VS_0, CS_{Str}, PS_{Str} and VS_{Str} (Fig. 5j, l).

For the PS_0 parameter, differences were found at small (PS_{0_S}) and medium (PS_{0_M}) scales (Fig. 5e). For example, the mean ± SDs of the CS_{Sta}, CS0, CS45, CS90 and CS_{Str}

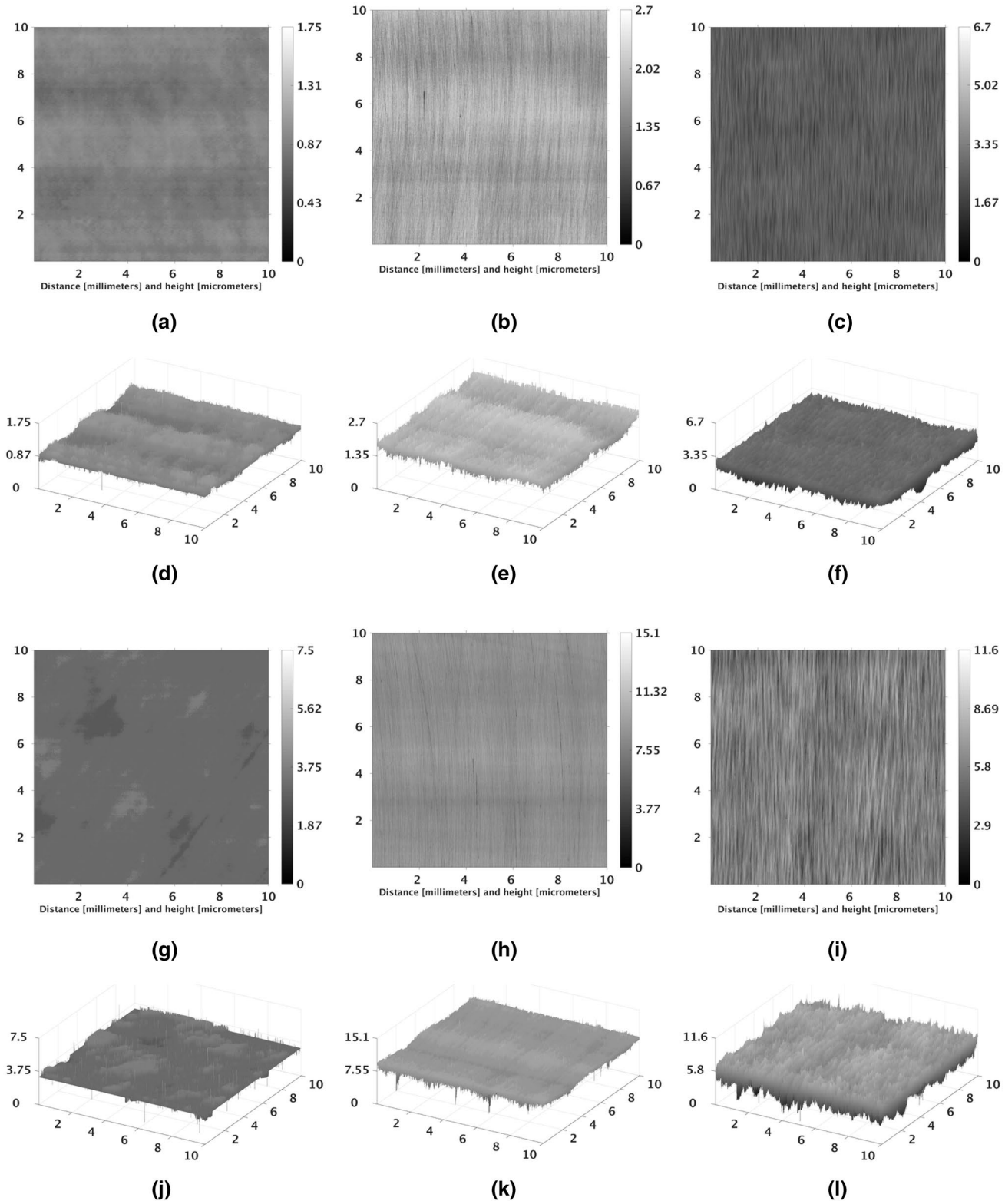

Fig. 4 Range-images and corresponding 3D views of **a**, **d** STE-S, **b**, **e** STE-A, **c**, **f** STE-R, **g**, **j** DLC-S, **h**, **k** DLC-A, and **i**, **l** DLC-R surfaces. Each image area is 10×10 mm

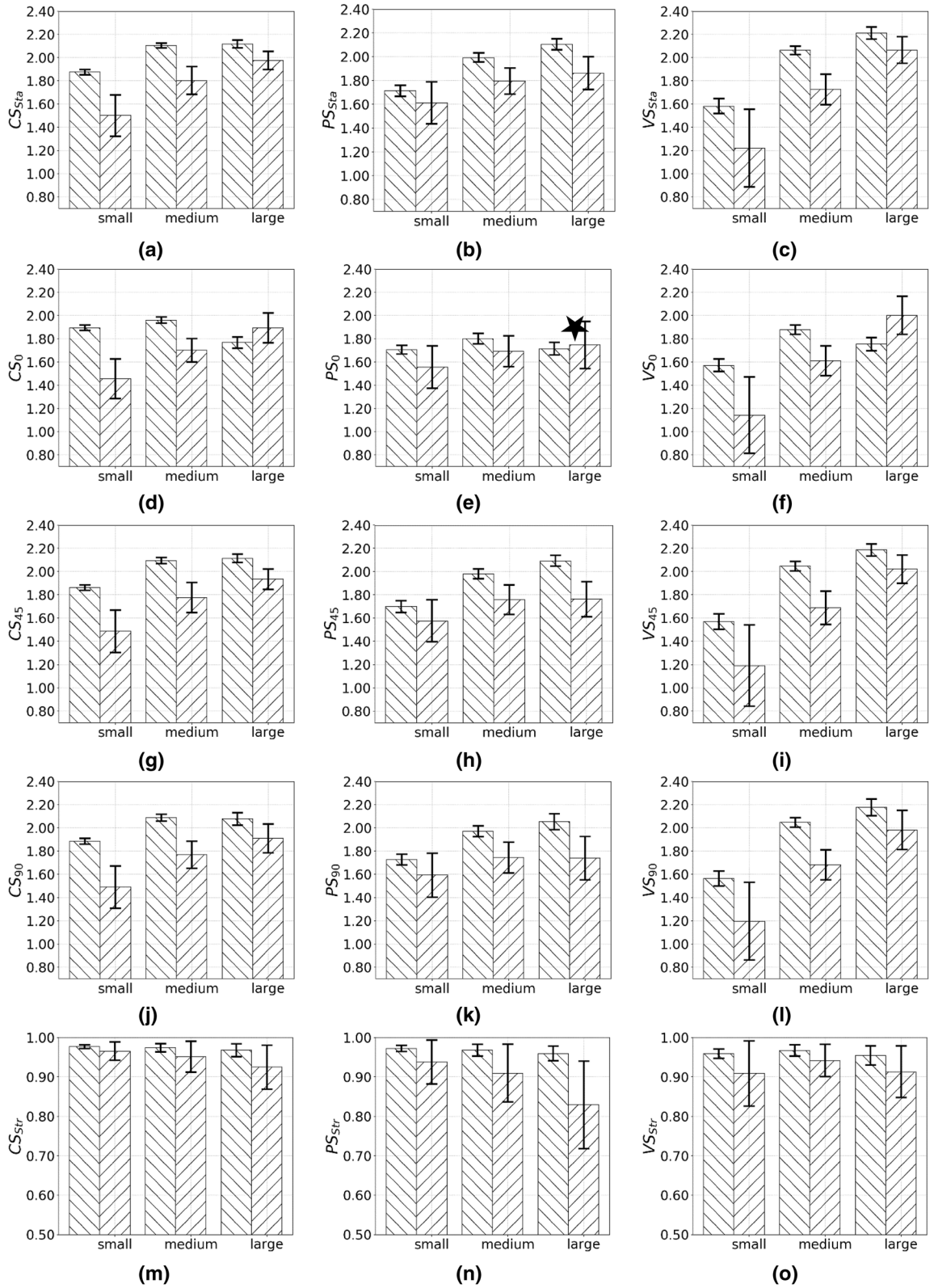

Fig. 5 Mean and SDs (error bars) of the CS, PS and VS calculated for the STE-S (diagonal-down lines) and DLC-S (diagonal-up lines) surfaces at small, medium and large scales. Non-significant differences ($P > 0.05$) are marked by a star

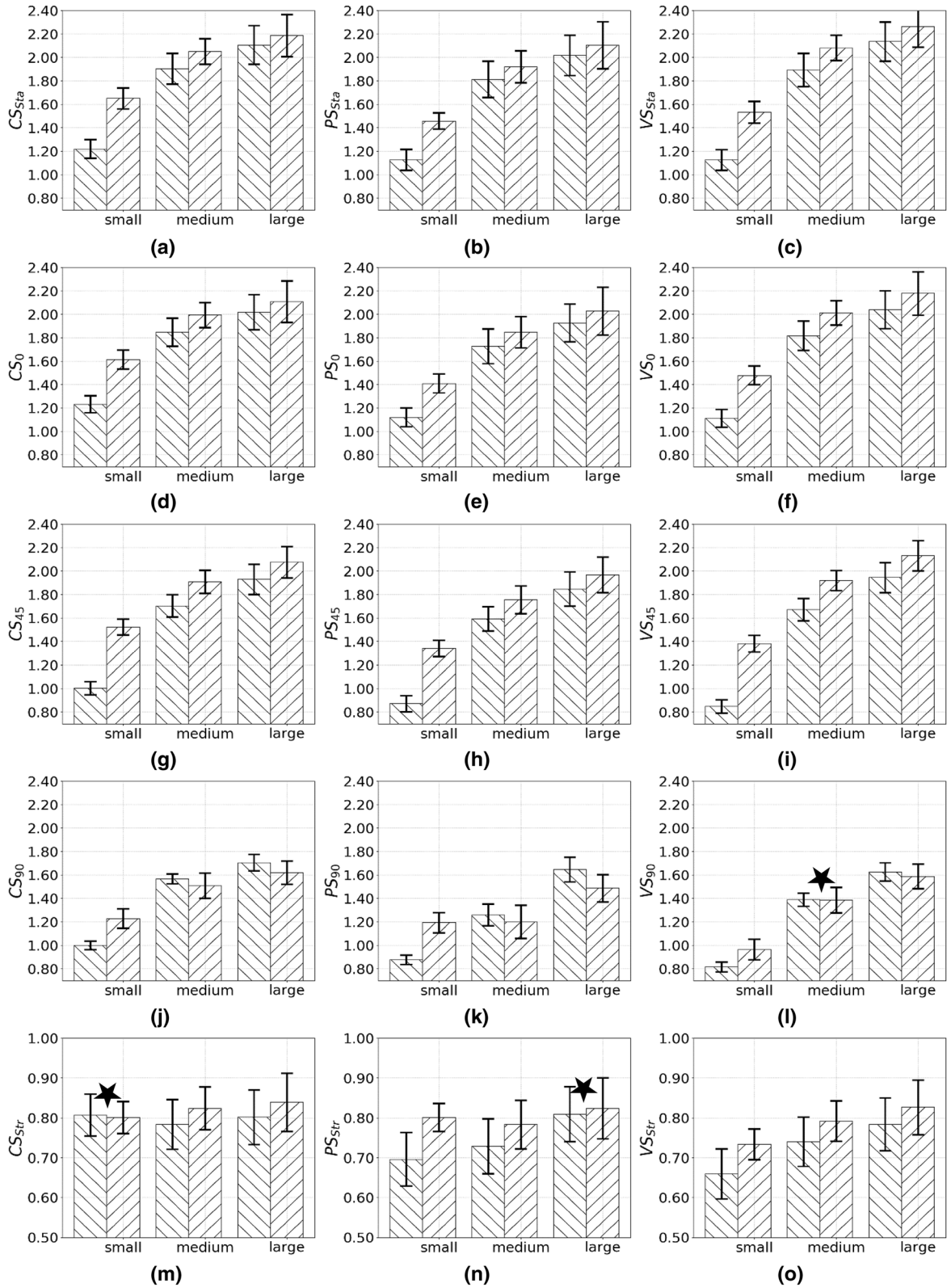

Fig. 6 Mean and SDs (error bars) of the CS, PS and VS calculated for the STE-A (diagonal-down lines) and DLC-A (diagonal-up lines) surfaces at small, medium and large scales. Non-significant differences ($P > 0.05$) are marked by a star

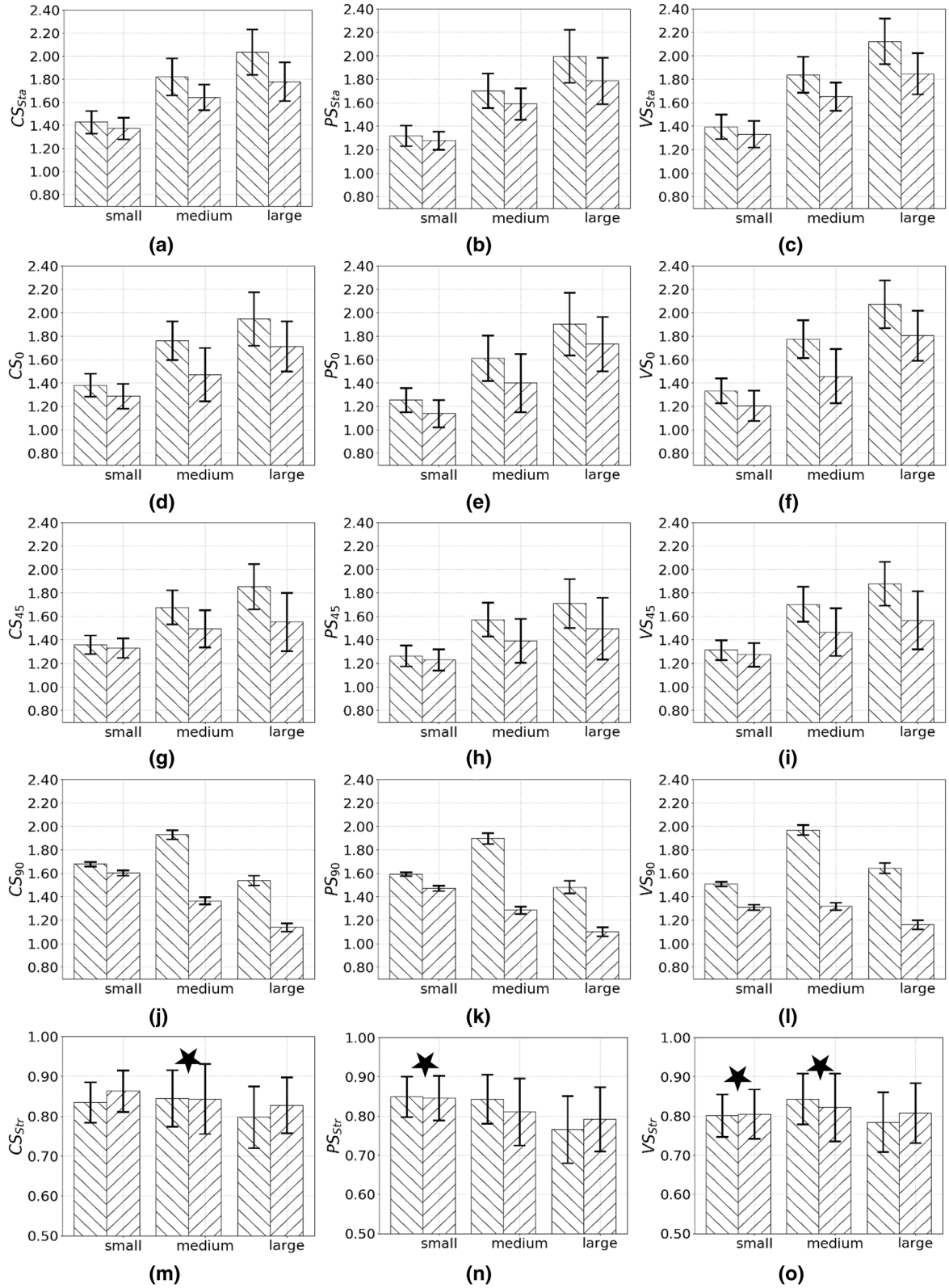

Fig. 7 Mean and SDs (error bars) of CS, PS and VS calculated for the STE-R (diagonal-down lines) and DLC-R (diagonal-up lines) surfaces at small, medium and large scales. Non-significant differences ($P > 0.05$) are marked by a star

obtained for the STE-S (DLC-S) surface at small scales are 1.877 ± 0.248 (1.501 ± 0.178), 1.900 ± 0.228 (1.456 ± 0.171), 1.864 ± 0.0238 (1.485 ± 0.182), 1.886 ± 0.0237 (1.490 ± 0.182), 0.977 ± 0.005 (0.965 ± 0.002), respectively.

3.2 STE-A and DLC-A Surfaces

As compared to the DLC-A, the CS, PS and VS obtained for STE-S surfaces in directions of dominating curvature complexity, 0° and 45°, were significantly lower ($P < 0.022$) at all scales (Fig. 6a–c, g–l). Examples of mean ± SDs values obtained for the uncoated surface are 1.220 ± 0.080 (CS_{Sta_S}), 1.231 ± 0.072 (CS_{0_S}) and 1.005 ± 0.057 (CS_{45_S}). For the coated surfaces, the values are 1.652 ± 0.090 (CS_{Sta_S}), 1.615 ± 0.081 (CS_{0_S}) and 1.523 ± 0.068 (CS_{45_S}). In the vertical direction, the CS, PS and VS obtained at medium and large scales for the STE-A surfaces (e.g. 1.567 ± 0.043 for CS_{90_M}) were higher than those for the DLC-A (e.g. 1.509 ± 0.108 for CS_{90_M}; Fig. 6j–l). The exception is the VS_{90_M} for which no differences were found (Fig. 6l).

The CS_{Str} (medium and large scales), PS_{Str} (small and medium scales) and VS_{Str} (all scales) calculated for the DLC-A surfaces were higher ($P < 0.010$) than those obtained for the STE-A surfaces (Fig. 6m–o). Example mean ± SDs values calculated for the CS_{Str_M} are 0.8241 ± 0.05392 (DLC-A) and 0.7838 ± 0.06232 (STE-A).

3.3 STE-R and DLC-R Surfaces

All parameters calculated at all scales for the STE-R surface were higher ($P < 0.031$) than those for the DLC-R surface (Fig. 7). The exceptions were CS_{Str_S}, CS_{Str_L}, PS_{Str_L} and VS_{Str_L} (Fig. 7m–o) which were higher for the coated surface, as compared to the uncoated surfaces. Examples of mean ± SDs values calculated for the STE-R surfaces are 1.428 ± 0.097 (CS_{Sta_S}), 1.382 ± 0.099 (CS_{0_S}), 1.3587 ± 0.080 (CS_{45_S}), 1.678 ± 0.017 (CS_{90_S}) and 0.8345 ± 0.05062 (CS_{Str_S}). For the DLC-R surfaces, the values are 1.372 ± 0.095 (CS_{Sta_S}), 1.286 ± 0.107 (CS_{0_S}), 1.399 ± 0.083 (CS_{45_S}), 1.603 ± 0.023 (CS_{90_S}) and 0.863 ± 0.052 (CS_{Str_S}).

No differences were detected for CS_{Str_M}, PS_{Str_S}, VS_{Str_S} and VS_{Str_M} (Fig. 7m–o).

4 Discussion

In this study, the recently developed DBCC method has been applied to images of uncoated and DLC-coated surfaces with increasing roughness and curvature. The method has a unique ability to precisely quantify a surface curvature complexity at individual scales and directions. Our study evidenced that the DBCC method detects minute differences in curvature between DLC-coated and uncoated surfaces. This suggests that the method has a potential to become a useful tool in design and optimization of such surfaces.

4.1 STE-S and DLC-S Surfaces

Curvature signatures calculated for the STE-S surfaces in the dominating curvature, 0°, 45° and 90° directions were higher than those for the DLC-S surfaces at all scales. The higher curvature complexity of the uncoated surfaces agrees with the higher roughness (higher values of FDs) of uncoated surfaces found in our previous study [8]. We reported in that study that the STE-S surfaces exhibit higher FDs than the DLC-S surfaces [8] and curvature complexity increases with FD [19]. Also, the density of summits (Sds) calculated for the STE-S surfaces are approximately twice higher than for the DLC-S surfaces.

Differences between the coated and uncoated surfaces were generally larger for the VS parameters as compared to the PS parameters. This suggests that valleys are a major contributor to the overall curvature complexity. To investigate this further, the peak and valley curvature matrices, i.e. the matrices generated in step 6 (Sect. 2.1 and Fig. 1f), were visually examined. Examples of the matrices obtained in the horizontal direction at scale of 30 µm are shown in Fig. 8b, c, e, f. The examination indicates that the matrices obtained for the DLC-S surfaces contain relatively flat large parts as compared to the STE-S surfaces. Also it was observed that the valley curvature matrices constructed for the DLC-S are sparser and the curvature values stored in these matrices are generally higher than those of peaks.

Coated surfaces were found to exhibit larger changes of curvature complexity with direction (i.e. more anisotropic) than the uncoated surfaces. This could be explained by the fact that the structure of DLC coating is heterogeneous, containing impurities [7]. This results in an uneven distribution of peaks and valleys on the coated disc. Peaks and valleys are almost evenly distributed on the STE-S surfaces (Fig. 8b, c), whereas the opposite is true for the DLC-S surfaces (Fig. 8e, f).

4.2 STE-A and DLC-A Surfaces

The CS, PS and VS parameters calculated for the average coated surfaces were higher than the uncoated surfaces in the dominating curvature complexity (all scales), 0° (all scales), 45° (all scales) and 90° (small scales) directions. The results showed that the coated surfaces exhibit a higher complexity of curvature than the uncoated in these directions. A possible explanation could be that the DLC-A surfaces are rougher (i.e. higher FDs) than the STE-A surfaces at small scales in the 0° and 45° directions

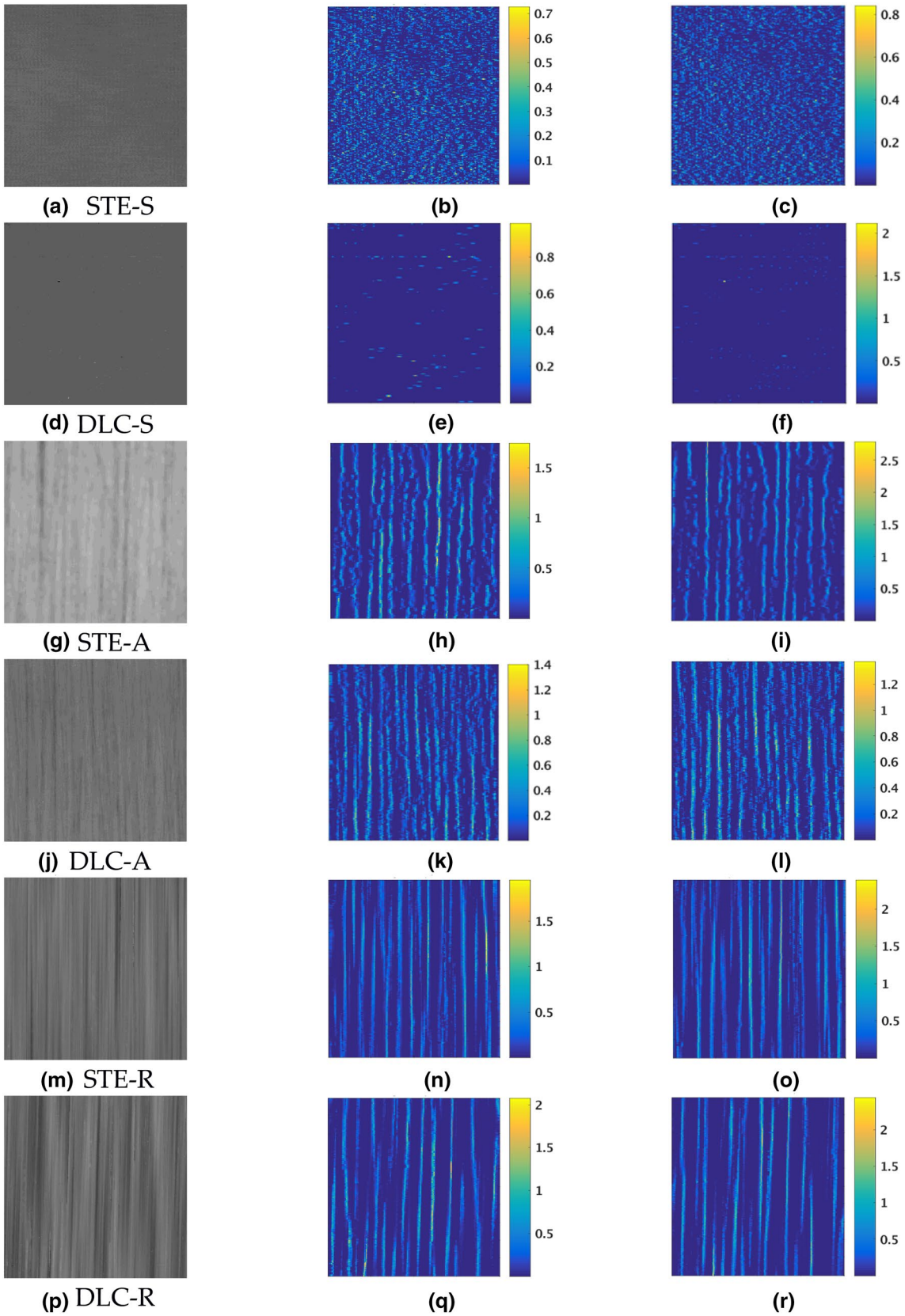

Fig. 8 Example sub-images of the **a**, **g**, **m** STE and **b**, **j**, **p** DLC surfaces and the corresponding visual representations of **b**, **e**, **h**, **k**, **n**, **q** peak and **c**, **f**, **i**, **l**, **o**, **r** valley curvature matrices obtained in the horizontal direction at the scale of 30 μm. The colour bars represent absolute values of the curvatures calculated

[8]. Also, the Sds obtained for the DLC-A disc was about ten times higher than for the STE-A disc.

Similar differences were found in the PS and VS parameters between STE-A and DLC-A surfaces. Visual examination of the peak and valley curvature matrices (Fig. 8h, i, k, l) shows that they are similar. These suggest that valleys and peaks have an approximately equal contribution to the overall curvature complexity of the coated and uncoated surfaces analysed.

Variation with direction in curvature complexity of the STE-A surfaces was higher than that of the DLC-A surfaces. This agrees with observation that the grinding marks deviate from the vertical direction more on the coated than on the uncoated discs, and also, the valley and peak curvature matrices exhibit uniform columnar patterns (Fig. 8h, i, k, l).

4.3 STE-R and DLC-R Surfaces

The CS, PS and VS parameters took higher values for the STE-R surfaces, as compared to the DLC-R surfaces. This agrees with our previous study showing that the uncoated surfaces are rougher than the coated surfaces [8], and the STE-R disc has the high values of Sds parameter.

Similar differences were detected between the STE-A and DLC-A surfaces using the PS and VS parameters. This indicates that valleys and peaks contribute approximately equally to the overall curvature complexity. This is further evidenced by the fact that peak and valley curvature matrices obtained for these two surfaces are similar (Fig. 8n, o, q, r).

No significant differences in the Str parameter were found between the rough coated and uncoated surfaces. The lack of changes of curvature with direction could be explained by the dominance of the vertical grinding marks. Visual examination of curvature matrices (Fig. 8n, o, q, r) obtained for these surfaces shows virtually same spatial distributions for peaks and valleys.

4.4 Limitations

The study conducted has some limitations. First, only a limited number of DLC-coated surfaces were analysed and only one type of DLC coatings was used (i.e. hydrogen-free DLC). It is unknown to what extent findings from this study could be generalized to other coatings (e.g. hydrogenated DLC [25]). Second, P-values calculated were not corrected for multiplicity. However, such correction could result in finding no differences where dissimilarities between coated and uncoated surfaces are present [26]. Third, the curvature parameters were calculated at three directions. Other directions might provide different results.

5 Conclusions

The following conclusions can be drawn from this study:

- Roughness and curvature of DLC-coated surfaces are difficult to characterize at individual scales and directions. The problem of the multiscale and directional roughness analysis of the coated surfaces has been addressed in our previous work using the DBC method. In the present work, a multiscale curvature characterization of the surfaces has been successfully completed using the DBCC method.
- The DBCC method is able to correctly detect minute differences in curvature at individual scales and in different directions between uncoated and DLC-coated bearing steel discs.
- The method can be used to assess contributions of surface features into the overall curvature complexity. It was found that peaks and valleys contribute approximately equally into the curvature complexity of average and rough coated and uncoated surfaces. For the smooth surfaces, valleys are a major contributor.
- Curvature directionality can be assessed using the DBCC method. Curvature of smooth coated surfaces exhibits greater changes with direction as compared to the uncoated surfaces. The opposite is true for the average surfaces. For the rough surfaces, there are no clear differences in curvature directionality.
- The detailed information about curvature provided by the DBCC method could be used to complement multiscale roughness analyses conducted using the DBC method. New relations between surface topography of DLC-coated surfaces and their wear and friction properties could be potentially found. This might be useful in designing of wear-resistant surfaces and tribological systems.

Acknowledgements The authors wish to thank Curtin University and the School of Civil and Mechanical Engineering for their support during preparation of the manuscript. The study was conducted as part of the Implementing Agreement on Advanced Material for Transportation Applications, Annex IV Integrated Engineered Surface Technology. The Implementing agreement functions within a framework created by the International Energy Agency (IEA). The views, findings and publications of the AMT IA do not necessarily represent the views or policies of the IEA or of all of its individual member countries.

References

1. Cabanettes, F., Claret-Tournier, J., Mohlin, J., Nilsson, P.H., Rosén, B.G., Xiao, L.: The evolution of surface topography of injection cams. Wear **266**, 570–573 (2009)

2. Mello, J., Binder, R., Demas, N., Polycarpou, A.: Effect of the actual environment present in hermetic compressors on the tribological behaviour of a si-rich multifunctional dlc coating. Wear **267**, 907–915 (2009)
3. Raulio, M., Jaarn, M., Ahola, J., Peltonen, J., Rosenholm, J., Tervakangas, S., Kolehmainen, J., Ruokolainen, R., Narko, P., Salkinoja-Salonen, M.: Microbe repelling coated stainless steel analysed by field emission scanning electron microscopy and physicochemical methods. J. Ind. Microbiol. Biotechnol. **35**, 751–760 (2008)
4. Suh, A., Polycarpou, A.: Effect of molecularly thin lubricant on roughness and adhesion of magnetic disks intended for extremely high-density recording. Tribol. Lett. **15**, 365–375 (2003)
5. Scibior, A., Adamczyk, A., Mroczka, R., Niedzwiecka, I., Golebiowska, D., Fornal, E.: Effects of vanadium (V) and magnesium (Mg) on rat bone tissue: mineral status and micromorphology. Consequences of V-Mg interactions. Metallomics **6**, 2260–2278 (2014)
6. Ray, S., Chowdhury, R.: S.K.R.: Experimental investigation into the effect of 3D surface roughness parameters on flash temperature. Ind. Lub. Tribol. **63**, 90–102 (2011)
7. Holmberg, K., Laukkanen, A., Ronkainen, H., Waudby, R., Stachowiak, G., Wolski, M., Podsiadlo, P., Gee, M., Nunn, J., Gachot, C., Li, L.: Topographical orientation effects on friction and wear in sliding DLC and steel contacts, part 1: experimental. Wear **330–331**, 3–22 (2015)
8. Wolski, M., Podsiadlo, P., Stachowiak, G., Holmberg, K., Laukkanen, A., Ronkainen, H., Gee, M., Nunn, J., Gachot, C., Li, L.: Multiscale characterisation of 3D surface topography of DLC coated and uncoated surfaces by directional blanket covering (DBC) method. Wear **388–389**, 47–56 (2017)
9. Laukkanen, A., Holmberg, K., Ronkainen, H., Stachowiak, G., Podsiadlo, P., Wolski, M., Gee, M., Gachot, C., Li, L.: Topographical orientation effects on surface stresses influencing on wear in sliding DLC contacts, Part 2: Modelling and simulations. Wear **388**, 18–28 (2017)
10. Wolski, M., Podsiadlo, P., Stachowiak, G.W.: Directional fractal signature analysis of trabecular bone: evaluation of different methods to detect early osteoarthritis in knee radiographs. Proc. Inst. Mech. Eng. Part H **223**, 211–236 (2009)
11. Wolski, M., Podsiadlo, P., Stachowiak, G.W.: Applications of the variance orientation transform method to the multiscale characterization of surface roughness and anisotropy. Tribol. Int. **43**, 2203–2215 (2010)
12. Wolski, M., Podsiadlo, P., Stachowiak, G.W.: Characterization of surface topography from small images. Tribol. Lett. **61**, 2 (2016)
13. Wolski, M., Podsiadlo, P., Stachowiak, G.W., Lohmander, L.S., Englund, M.: Differences in trabecular bone texture between knees with and without radiographic osteoarthritis detected by directional fractal signature method. Osteoarthr. Cartil. **18**, 684–690 (2010)
14. Wolski, M., Stachowiak, G.W., Dempsey, A.R., Mills, P.M., Cicuttini, F.M., Wang, Y., Stoffel, K.K., Lloyd, D.G., Podsiadlo, P.: Trabecular bone texture detected by plain radiography and variance orientation transform method is different between knees with and without cartilage defects. J. Orthop. Res. **29**, 1161–1167 (2011)
15. Podsiadlo, P., Nevitt, M.C., Wolski, M., Stachowiak, G.W., Lynch, J.A., Tolstykh, I., Felson, D.T., Segal, N.A., Lewis, C.E., Englund, M.: Baseline trabecular bone and its relation to incident radiographic knee osteoarthritis and increase in joint space narrowing score: directional fractal signature analysis in the MOST study. Osteoarthr. Carti. **24**, 1736–1744 (2016)
16. Wolski, M., Podsiadlo, P., Stachowiak, G.W.: Directional fractal signature analysis of self-structured surface textures. Tribol. Lett. **47**, 323–340 (2012)
17. Podsiadlo, P., Wolski, M., Stachowiak, G.W.: Fractal analysis of surface topography by the directional blanket covering method. Tribol. Lett. **59**, 41 (2015)
18. Brown, C.A., Hansen, H.N., Jiang, X.J., Blateyron, F., Berglund, J., Senin, N., Bartkowiak, T., Dixon, B., Le Goic, G., Quinsat, Y., Thompson, W.J.,S., Ungar, M.K., Zahouani, P.S.: E.H.: Multiscale analyses and characterizations of surface topographies. CIRP Ann. **67**, 839–862 (2018)
19. Podsiadlo, P., Wolski, M., Stachowiak, G.: Novel directional blanket covering method for surface curvature analysis at different scales and directions. Tribol. Lett. **65**, 2 (2017)
20. Geraets, W.G.M.: Comparison of two methods for measuring orientation. Bone **23**, 383–388 (1998)
21. Bryan, J.B.: The Abbe principle revisit: an updated interpretation. Prec. Eng. **1**, 129–132 (1979)
22. Whitehouse, D.J.: Handbook of Surface and Nanometrology, 2edn. CRC Press, Boca Raton (2010)
23. Chernov, N., Ma, H.: Least squares fitting of quadratic curves and surfaces. In: Yoshida, S.R. (ed.) Computer Vision, 2edn., pp. 285–302. Nova Science Publishers, San Francisco (2011)
24. Faul, F., Erdfelder, E., Lang, A.G., Buchner, A.: G*Power 3: a flexible statistical power analysis program for the social, behavioral, and biomedical sciences. Behav. Res. Methods **39**(2), 175–191 (2007)
25. Ronkainen, H., Varjus, S., Koskinen, J., Holmberg, K.: Differentiating the tribological performance of hydrogenated and hydrogen-free DLC coatings. Wear **249**, 260–266 (2001)
26. Ranstam, J.: Multiple p-values and Bonferroni correction. Osteoarthr. Cartil. **24**, 763–764 (2016)